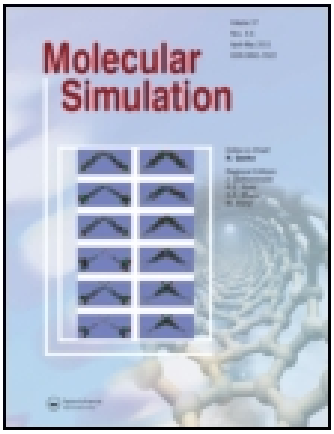

Molecular Simulation
Publication details, including instructions for authors and subscription information:
http://www.tandfonline.com/loi/gmos20

Structural Modelling of Vanadium Pentoxide

A. Dietrich [a] , C. R. A. Catlow [b] & B. Maigret [c]

[a] Laboratoire de Modélisation Moléculaire , 12 rue Adalbert de Baerenfels, 68300, Saint-Louis, Bourgfelden, France

[b] The Royal Institution of Great Britain , 21 Albemarle Street, London, WIX4BS, UK

[c] Laboratoire de Chimie Théorique, URA CNRS 510, Université de Nancy I , B.P. 239, 54506, Vandœuvre, Cédex, France

Published online: 23 Sep 2006.

To cite this article: A. Dietrich , C. R. A. Catlow & B. Maigret (1993) Structural Modelling of Vanadium Pentoxide, Molecular Simulation, 11:5, 251-265, DOI: 10.1080/08927029308022513

To link to this article: http://dx.doi.org/10.1080/08927029308022513

Molecular Simulation, 1993, Vol. 11(5), pp. 251-265
Reprints available directly from the publisher
Photocopying permitted by license only

STRUCTURAL MODELLING OF VANADIUM PENTOXIDE

A. DIETRICH*

Laboratoire de Modélisation Moléculaire, 12 rue Adalbert de Baerenfels, 68300 Saint-Louis Bourgfelden, France

C.R.A. CATLOW

The Royal Institution of Great Britain, 21 Albemarle Street, London WIX4BS, UK

B. MAIGRET

Laboratoire de Chimie Théorique, URA CNRS 510, Université de Nancy I, B.P. 239, 54506 Vandœuvre Cédex, France

(Received January 1993, accepted January 1993)

Computational techniques, based on the minimization of the crystal energy with respect to atomic coordinates, are shown to predict correctly the complexity of the V_2O_5 crystal structure. Two main types of potential are derived, both fitted to the experimentally determined structure. One is based on integral ionic charges, the other uses partial charges. In all cases the deviations of the observed structures from the ideal model based on regular VO_6 octahedra is correctly reproduced by the energy-minimization techniques. We also qualitatively reproduce some of the important macroscogic properties of this material.

KEY WORDS: Potential model, atomistic simulation, vanadium pentoxide, ionic polarization

INTRODUCTION

Computer simulation techniques have been applied to a wide range of structure problems in the field of complex and disordered ionic solids [1]. Early applications to inorganic materials were reported by Slaughter [2] and by Busing [3]. Catlow, Theobald & Cormack [4] showed that energy-minimization could be used as predictive tools and the methods have subsequently been extensively applied to the modelling of complex inorganic crystal structures given knowledge of the relevant interatomic potentials and general structural informations such as the nature and the linkage of the coordination polyhedra. A recent review is given in reference [5].

The simulation techniques rest on the Born model of the ionic solid and are based on energy minimization, **either of** the coordinates of ions within the unit cell of a

* to whom all correspondence should be sent

perfect crystal structure **or of** ion coordinates around a defect centre. The former technique will be intensively employed in this work which will be concerned with the highest vanadium oxide, V_2O_5. This oxide is commonly employed in catalytic processes and is of considerable interest as a cathodic material in ambient temperature secondary cells [6]. The latter method will be used for studies of alkali metal insertion into the host structure V_2O_5. Numerous ternary compounds (so called because three species are involved in the final product) of the general form $M_xV_2O_5$ ($M = Li^+$, Na^+, Cu^+, K^+) have been synthesised. They are more commonly known as "bronzes" because of the bronze colour taken by the compound as the percentage of M increases. Depending on the degree of insertion (x) and the temperature of synthesis, six distinct crystallographic phases have been exhibited for the $Li_xV_2O_5$ system [7, 8, 9, 10, 11]. At ambient temperature there are only two phases: from $x = 0$ up to $x = 0.8$ there is an increase of the gap between the slabs, corresponding to a 10% increase in the c lattice parameter; while for $0.8 < x < 1.0$ the slabs pucker and shift above each other by half an octahedron thus giving the metastable form $Li_{0.9}V_2O_5$-δ [12]. A detailed review of these materials synthesised by both chemical and electrochemical means is available in *Intercalation Chemistry* [13]. Full understanding of these systems will require an extensive series of calculations which will be reported subsequently.

Before these and related systems can be studied it is essential to derive adequate interatomic potentials. Several computer simulation studies have been performed on transition-metal oxides and potential models are available for several systems. However, the only existing potential for vanadium oxides concerns the rutile-structured VO_2 [14], which was applied succesfully to the B phase of VO_2 [15] but gave poor results once transfered to the V_2O_5 structure. We analyse here the reasons for this failure and propose a new set of interatomic potentials specifically well suited to the layered structure of V_2O_5.

THE STRUCTURE OF V_2O_5

The first structural investigation of the V_2O_5 structure was performed by Ketelaar in 1936 [16]. Later, Byström, Wilhelmi & Brotzen [17] proposed the structural description based on trigonal bipyramids sharing edges and corners, making V_2O_5 sheets. Enjalbert & Galy [18] reported a detailed structural study of this oxide and concluded that the oxygen coordination polyhedron around the Vanadium atom should be described in terms of a **square pyramid** instead of a trigonal bipyramid. The base of the pyramid is quasi planar, $\angle(O_{21}O_{31}O_{23})/(O_{21}O_{31}O_{23}') = 1.4°$, and the distances of the four atoms of the base to the average plane are less than 0.014 Å. The Vanadium atom is displaced from this plane by 0.47 Å, the cause of which is not yet fully elucidated. It appears that the Vanadium atom can be easily displaced within its anion polyhedron [19]. This anisotropic behavior leads to three interesting properties:

(i) The V atom is displaced toward the apex of the square pyramid creating a strong vanadyl bond $\mathbf{V = O_{11}}$ of length 1.577 Å. The opposite $V\text{-}O_{11}$ bond is then lenghened to 2.791 Å.
(ii) The V^{5+}-V^{5+} repulsion causes the square VO_5 pyramids sharing edges to have **opposite orientations** [20].

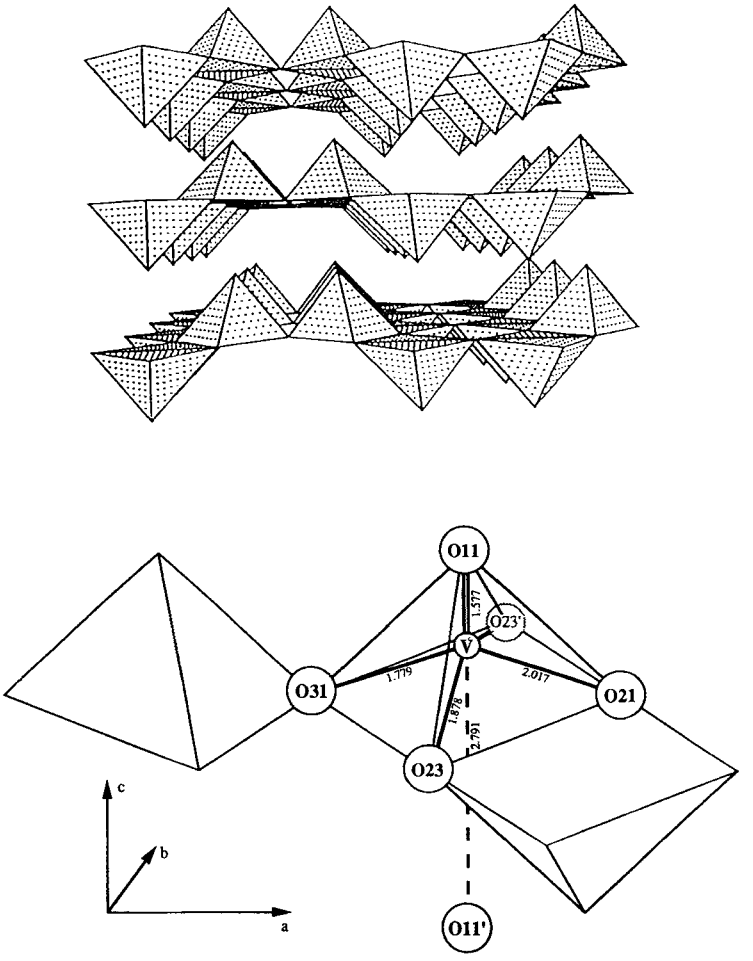

Figure 1 Definition of the coordinate system and atom labelling.

(iii) the long V ... O_{11} bond cannot be described as a covalent bond, as the structure can be easily intercalated by various molecular compounds. The layers are held together by weak van der Waals forces.

On figure 1 we can see that square pyramids share edges and extend along the *b* axis forming a zig-zag ribbon. These ribbons are joined together via the O_{31} atom, making V_2O_5 sheets.

The appearance of sheets in V_2O_5 is attributable to the anisotropy of the V position relative to its oxygen environment. When looking along the *c*-axis, we can see an anion/cation sequence as shown in Figure 3a.

It is of interest to compare V_2O_5 with another important layer structured solid TiS_2, in which reversible lithium insertion is also possible and whose structure is shown in Figure 2. Titanium atoms are held between hexagonally close-packed

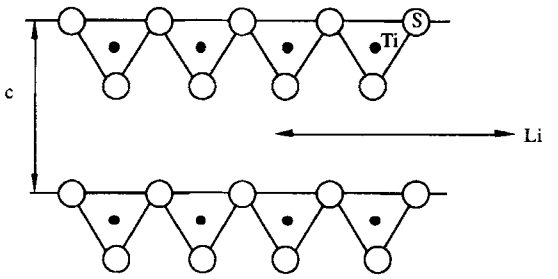

Figure 2 Schematic structure of TiS_2 layers.

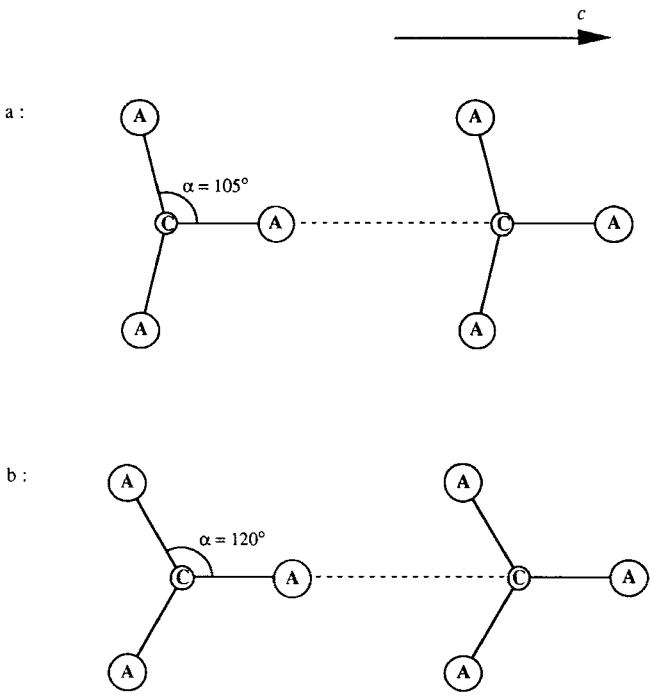

Figure 3 Sequence of Anion and Cation in layered compounds.

sulphur atoms to form layers which are held together by weak van der Waals forces [21]; the sequence is shown in Figure 3b.

The TiS_2 structure corresponds more to a packing of elementary slabs than does that of V_2O_5. However, when lithium is inserted it may approach closer to the V cation in V_2O_5 than the Ti cation in TiS_2. Thus the role of the cation in the intercalation process seems more important in V_2O_5 than in TiS_2.

A further important feature of the structure concerns the polyhedron linkage which it is important to understand when we wish to determine the position of the atoms in the ideal V_2O_5 structure based on regular octahedra. Starting from a

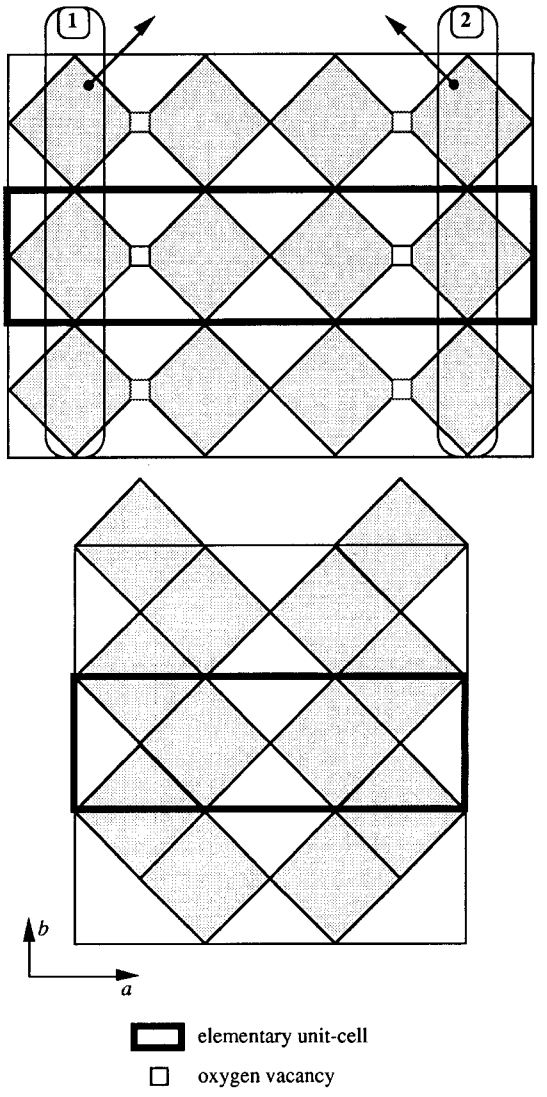

Figure 4 The VO_3 to V_2O_5 transition.

hypothetical VO_3 structure similar to ReO_3, where octahedra link up at their corners to form a three-dimensional framework, we can create an extended defect by removing a complete line of Oxygen atoms (Figure 4). When removing one such line out of two, the structure has to rearrange to fill the vacancies. The chains 1 and 2 can move along a diagonal direction in order to create the edge shared octahedra; then we reproduce the topology of the V_2O_5 structure. V_2O_5 is now viewed as a **crystallographic shear** structure derived from VO_3, by the mechanism first proposed by Wadsley [22, 23], which results in all of the oxygen deficiency

being concentrated within these crystallographic shear planes. These planes separate regions of normal rutile structure and can then explain the evolution of oxygen-defficiency in the homologous series of Magneli phases M_nO_{2n-1} (M = Ti, V, Mo and n = 3, . . ., 10) [24].

COMPUTATIONAL METHODS

A preliminary model, based on regular coordination polyhedra is choosen as an initial structure in our minimization calculations. Starting from this ideal model, the lattice energy is minimized with respect to the coordinates of all atomic positions within the unit cell.

The interatomic potential is based on the ionic model. Thus, the lattice energy is expressed as a sum of pair-wise interactions represented by the function:

$$V_{ij}(r) = A_{ij}\exp(-r/\rho_{ij}) - C_{ij}/r^6 + \frac{q_i q_j}{r}.$$

Here we use a Buckingham potential for the short-range interactions and a Coulombic term to handle the electrostatic effects. These long-range interactions are treated using the widely applied Ewald method [25] (a good description of which is given by Tosi [26]) which takes advantage of the rapid convergence of lattice sums for a Gaussian charge distribution when these are summed in reciprocal space. In the present study we have used first a rigid-ion model, *i.e.* one that excludes any treatment of ionic polarization from our calculations. This approximation may limit the accuracy of our results, although we believe, in general, that polarizability has a relatively minor effect on structural properties. Polarization can be incorporated into our calculations *via* the shell model of Dick & Overhauser [27] as has been done extensively in previous studies. Inclusion of this model, of course, be essential when a correct description of the dielectric properties is needed as, for example, when considering charged point defects.

An important feature of our method is that no explicit symmetry relations between the various atomic positions are assumed : all the coordinates are treated as independant variables in the minimization process and their relaxations are determined solely by the interatomic potentials and the unit-cell parameters. The limitations on the reliability of the technique follow only from those of the interatomic potentials used in the simulations [28] and from the approximations inherent in the static lattice method. We note that static dielectric constants have not been used in the fitting process; nor have the elastic constants, although these provide a valuable test of potential models, as no experimental values are presently available [29]. However the complex, low symmetry structure provides a good test of the quality of our potentials.

Efficient minimization methods are essential if the calculations are to be computationally viable. The methods employed in the perfect lattice part of the CASCADE code [30] are based on an adaptation of the Newton-Raphson procedure, with the update of the Hessian matrix, following the approach of Fletcher & Powell [31]. In the present sudy, cell dimensions were allowed to vary. This *constant pressure* minimization procedure places greater demands on the reliability of the interatomic potentials than a *constant volume* simulation.

POTENTIALS PARAMETERS

Three sets of potentials parameters have been derived:

- in set [A], integral ionic charges are used to the cation and the anion;
- in set [B], a more realistic charge distribution is proposed. Partial charges are placed on the cation and the anion, with the condition that the cell remains electroneutral;
- the third set [C] has been derived from [A] and integral ionic charges are also employed; but here the shell model is used to the oxygen ions so as to calculate the high frequency dielectric constants.

Part of the motivation for the development of the partial charge model is provided by the recent NMR studies on V_2O_5 [32] where the authors used partial charges [33] to compute the components of the electrical field gradient at the ^7Li nucleus. Integral charge models do, however, have advantages when considering the reduction of V_2O_5 which can easily be modelled by a V^{5+} to V^{4+} transition; this will be especially useful in future simulations of e.g. the γ-$Li_{1.0}V_2O_5$ phase where the location of the V^{4+} and V^{5+} ions is well established [9]. However, it is still possible to undertake calculations on reduced species with partial charge models. Thus a transition from +3.56 to +2.56 was also proposed by Cocciantelli *et al.* [32]. It seems useful therefore to derive models based on both partial and formal charges.

Parameters for the Vanadium/Oxygen short-range interactions have been fitted to the structure, while potential for the O–O interaction are taken from the work of Catlow on UO_2 [34]. V–V interactions are assumed to be purely coulombic; since the vanadium cation is smaller than the oxygen ion and the O–O interaction already very small at equilibrium lattice spacings this assumption seems to be reasonable. The attractive r^{-6} term is ignored in the V–O interactions; the small contribution of such terms to the short-range potential at the lattice interatomic spacings will be incorporated by small modifications of the A and ρ parameters [35]. All potential parameters are reported in Table 1. A major problem arose with the treatment of the vanadyl bond $V = O_{II}$ which is 1.577 Å long in one direction and 2.791 Å in the opposite direction. The ideal way to cope with this situation would have been to fix a unique set of repulsive parameters for $V\text{-}O_{II}$ and let the repulsion $V^{5+}\text{-}V^{5+}$ generate this anisotropy. However, this did not prove to be tractable. So we employed two different functions, one applied to $V = O_{II}$ and the other to $V \ldots O_{II}$. In view of the strength of the largely covalent vanadyl bond [36] we decided to apply a Morse function between these two species. The analytic form of the Morse potential is:

$$V(r) = D_e \left[1 - e^{(-\lambda(r - r_0))}\right]^2$$

(from which D_e should be substracted in order to be consistent with the other potentials which have the energy zero at infinity). The well depth was chosen by comparison to other strong double bonds [37]. We must note the derived value of r_0 which is greater than the expected experimental value of 1.577 Å. The effect is to displace the minimum of the function to the right to compensate for the Coulombic interaction between the Vanadium and Oxygen. This effective Morse potential should only deal with neutral species; but considering the importance of Electrostatic interactions in the cohesion of this layered compound, our calculation must integrate the Coulombic repulsion between Oxygen/Oxygen and the

Table 1 Potential parameters for V_2O_5.

SET	[A]	[B]	*[C]*		
Charge on Vanadium	+5	+3.56	*+5*	constant/eA Å^{-2}	*+0.717*
Charge on Oxygen	−2	−1.424	core		*−2.717*
			shell		*54.952*
			spring		
Buckingham Interaction		*A*/eV	*ρ*/Å	*C*/eV Å^{+6}	range/Å
		3000.0	**0.36415**	**0.0**	**1.99-3.0**
$V-O_{II}$		3374.32	0.32615	0.0	1.99-3.0
		2549.73	*0.34115*	*0.0*	*1.99-3.0*
		2779.85	**0.29185**	**0.0**	**0.0-10.0**
V-O		2419.85	0.2678	0.0	0.0-10.0
		5312.99	*0.26797*	*0.0*	*0.0-10.0*
		22764.3	**0.1490**	**23.0**	**0.0-10.0**
$O_{II}-O_{II}$, O-O, $O-O_{II}$		22764.3	0.1490	23.0	0.0-10.
		22764.3	*0.1490*	*23.0*	*0.0-10.0*
Morse Interaction		D_e/eV	λ/Å^{-1}	r_0/Å	range/Å
		10.0	**2.30217**	**1.774**	**0.0-1.99**
$V-O_{II}$		10.0	2.30217	1.706	0.0-1.99
		10.0	*2.30217*	*1.584*	*0.0-1.99*

Coulombic attraction between the Vanadium and the Oxygen of the upper layer. This can only be achieved by treating charged species.

These sets of potentials are clearly tailored to the V_2O_5 structure especially to the unusual structural properties of the Vanadium inside its oxygenated polyhedron which results in a range of interatomic V-O distances. The transferability to other vanadium oxides must therefore be questionable.

RESULTS AND DISCUSSION

The coordinates of the equilibrated and observed structures are reported in Table 2. As remarked earlier the minimization was performed at constant pressure which results in small differences between the calculated and X-ray lattice parameters. Thus a comparison of calculated and experimental fractionnal atomic coordinates is not strictly valid. We therefore convert all particle coordinates into Cartesian space and centre each unit-cell before calculating the differences between simulation and experience. We also report the discrepancies between lattice parameters of predicted and ideal structures to underline the magnitude of the distortion. We reproduce the experimental angle/distance table from Enjalbert [18] and we use the same presentation for the predicted structure in Table 3. Table 4 summarizes other calculated properties.

Figure 5 is a view along the *b* axis of the ideal structure (red facets) and the predicted one (yellow lines). Figure 6 is a comparison of the experimentally determined structure (red facets) - displayed with the 90% probability thermal ellipsoids - and the predicted structure (yellow lines). Figure 7 is the same comparison but the superposed structures are viewed along the *c* direction. The display has been performed on a raster graphic system [38].

Table 2 Structural parameters for V_2O_5.

	Idealized structure	*X-ray structure*	*Predicted structure**	Δ_1/%	Δ_2/%
		LATTICE PARAMETERS/Å			
a	12.00	11.512145	11.527921	0.137	−3.933
b	4.000	3.563922	3.473661	−2.532	−13.158
c	4.000	4.367690	4.367861	+0.004	+9.196

COORDINATES**

	X-ray structure			Predicted structure			
	x	*y*	*z*	*x*	*y*	*z*	Δ_3/Å
V	−4.5913	−0.8910	1.7108	−4.5976	−0.8684	1.7110	0.0234
V	4.5913	0.8909	−1.7108	4.6451	0.8684	−1.4059	0.3104
V	−1.1648	−0.8910	1.7108	−1.1189	−0.8684	1.7110	0.0511
V	1.1648	0.8909	−1.7108	1.1664	0.8684	−1.4059	0.3057
O_1	−4.5548	−0.8910	0.1344	−4.5655	−0.8684	0.1339	0.0249
O_1	4.5548	0.8909	−0.1344	4.6129	0.8684	0.1712	0.3119
O_1	−1.2012	−0.8910	0.1344	−1.1510	−0.8684	0.1339	0.0550
O_1	1.2012	0.8909	−0.1344	1.1985	0.8684	0.1712	0.3064
O_2	−4.9626	0.8909	2.1727	−5.1471	0.8684	2.1447	0.1879
O_2	4.9626	−0.8910	−2.1728	5.1946	−0.8684	−1.8395	0.4066
O_2	−0.7935	0.8909	2.1727	−0.5694	0.8684	2.1447	0.2269
O_2	0.7935	−0.8910	−2.1728	0.6168	−0.8684	−1.8396	0.3777
O_3	−2.8780	−0.8910	2.1891	−2.8582	−0.8684	1.9421	0.2488
O_3	2.8780	0.8909	2.1785	2.9057	0.8684	2.7312	0.5538

* Structure minimized in force field [B].
** Coordinates in cartesian space after centering about the origin.
Δ_1 Difference between the predicted and the X-rays lattice parameters.
Δ_2 Difference between the predicted and the idealized lattice parameters.
Δ_3 Distance between experimental and predicted position.

Table 3 Selected distances/Å and angles/°. **Experimental** and *Predicted**.

V	O_{11}	O_{31}	O_{23}	$O_{23'}$	O_{21}	$O_{11'}$
O_{11}	**1.577**	**2.652**	**2.738**	**2.738**	**2.868**	**4.368**
	1.577	*2.486*	*2.720*	*2.720*	*2.976*	*4.368*
	[0.00]	[−6.24]	[−0.67]	[−0.67]	[+3.77]	[0.00]
O_{31}	**104.3**	**1.779**	**2.742**	**2.742**	**3.671**	**2.857**
	96.407	*1.755*	*2.880*	*2.880*	*3.524*	*3.077*
	[−7.57]	[−1.37]	[+5.05]	[+5.05]	[−4.00]	[+7.70]
O_{23}	**104.5**	**97.1**	**1.878**	**3.564**	**2.386**	**2.961**
	103.744	*105.092*	*1.873*	*3.474*	*2.138*	*2.986*
	[−0.72]	[+8.23]	[−0.29]	[−2.53]	[−10.40]	[+0.83]
$O_{23'}$	**104.5**	**97.1**	**143.2**	**1.878**	**2.386**	**2.961**
	103.744	*105.092*	*136.091*	*1.873*	*2.138*	*2.986*
	[−0.72]	[+8.23]	[−4.96]	[−0.29]	[−10.40]	[0.83]
O_{21}	**105.2**	**150.5**	**75.5**	**75.5**	**2.017**	**3.050**
	116.389	*147.204*	*68.642*	*68.642*	*1.919*	*2.650*
	[+10.64]	[−2.19]	[−9.08]	[−9.08]	[−4.88]	[−13.12]
$O_{11'}$	**177.9**	**73.7**	**75.9**	**75.9**	**76.9**	**2.791**
	178.172	*81.765*	*76.806*	*76.806*	*65.439*	*2.792*
	[+0.15]	[+10.94]	[+1.19]	[+1.19]	[−14.90]	[+0.02]

* Structure minimized in force field [B].

Table 4 Comparison of experimental and calculated crystal data for V_2O_5.

PROPERTY		*Calculated*			*Experiment*
		[A]	*[B]*	*[C]*	
Lattice Energy/eV		−387.2	−208.9	−387.2	[−410.4 . . . −395.2]
Static dielectric constants	$\varepsilon_{0\|a}$	6.48	6.32	5.46	25.5
	$\varepsilon_{0\|b}$	13.57	34.92	10.05	15.0
	$\varepsilon_{0\|c}$	1.92	1.92	2.14	5.0
High dielectric constants	$\varepsilon_{\infty\|a}$			2.10	n_a^*:2.07(0.62)**
	$\varepsilon_{\infty\|b}$			2.28	n_b:2.12(0.61)
	$\varepsilon_{\infty\|c}$			1.57	n_c:1.97(0.71)

* Refractive indices.
** In parenthesis is $(n - \sqrt{\varepsilon_\infty})$

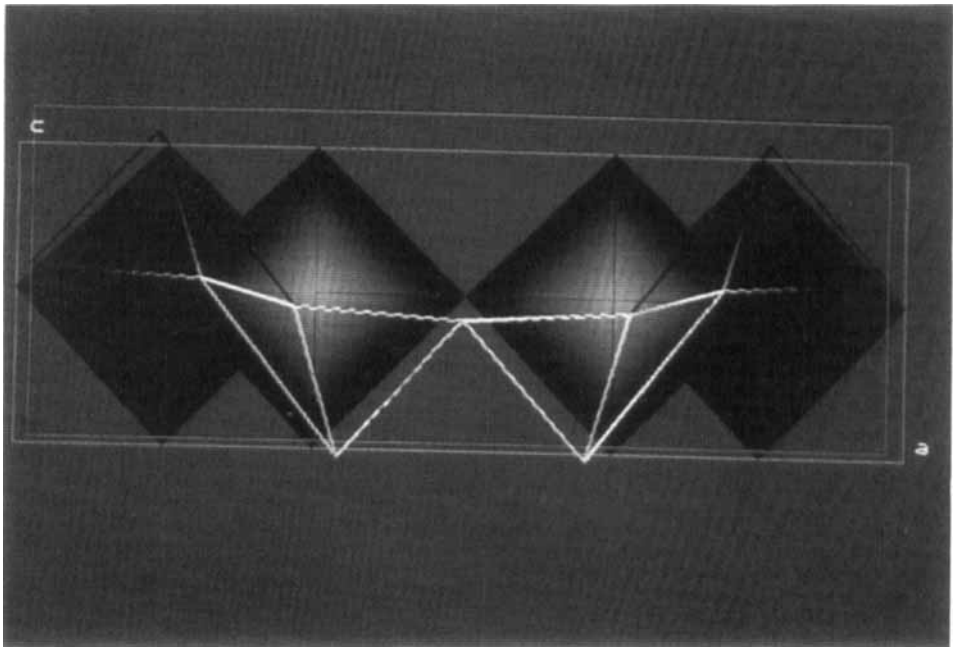

Figure 5 View along the *b* axis of the ideal structure (red facets) and the predicted one (yellow lines). (See Colour Plates)

The structural feature of major concern in the present study is the extent to which the observed structure differs from the ideal model. That such distortions are considerable is seen on figure 5 by comparing the parallelepiped (green for the ideal, red for the predicted) representing the orthorhombic unit-cell of the structures. On examining figure 6 we note that all atoms lie within their thermal ellipsoid. **Secondly**, the sheets of the predicted structure look more puckered than those of the X-ray structure. This is due to the shortening of the $V\text{-}O_{31}$ distance. A single V − O potential is applied to deal with the four square base oxygens and there is

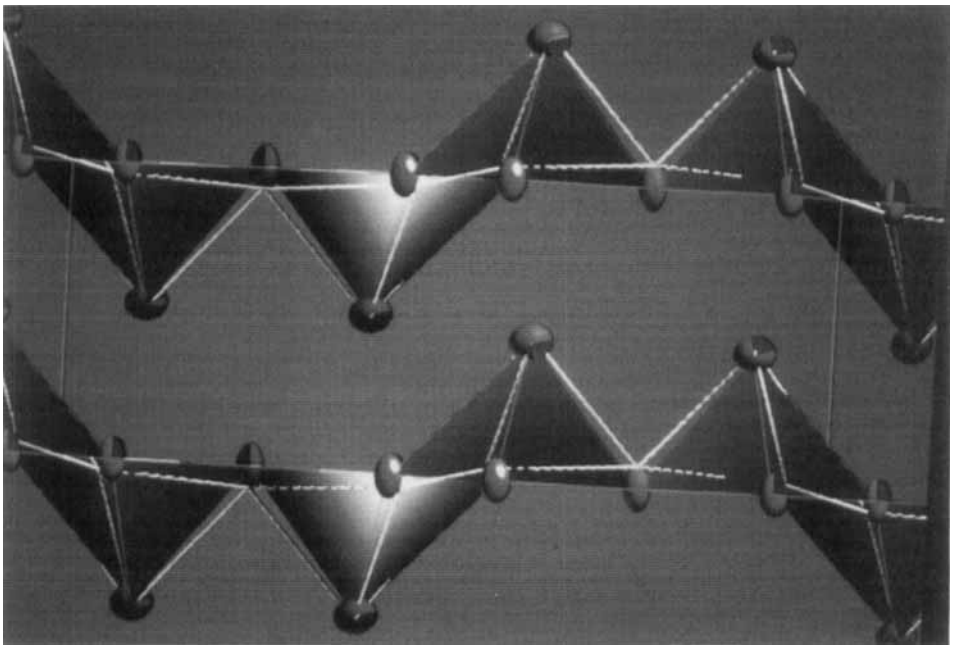

Figure 6 Comparison of the experimentally determined structure (red facets) and the predicted structure (yellow lines). (See Colour Plates)

a wide range of interatomic distances in this region, from 1.779 Å to 2.017 Å; this potential tends to gather the predicted distances around a mean value, so the experimental extrema are not reproduced accurately. Even so, the evolution along the diagonal of Table 3 (bold *vs.* italic) is preserved. A possible solution would be to apply a distinct repulsive form for each oxygen of the square base. This was not attempted because the increase in the number of parameters made the fitting process more hazardous. **Thirdly**, all the predicted Vanadium-Oxygen distances, and especially $V-O_2$ and $V-O_3$, are lower or equal to the observed one; so we might expect the predicted *a* lattice parameter to be lower than the observed one. This is, however, not the case. The only explanation resides in the bond angle distribution. The agreement between observed and predicted bond angles is far less good than for bond lengths. The $\angle O_{31}/O_{23}$ and $\angle O_{23}/O_{21}$ angles greatly influence the value of *a*; in the predicted structure their sum is greater than in the experimental one. **Fourthly**, the major structural difference between the structure predicted in force field [A] and [B] is the shortening of the O_{21}-O_{23} bond - the common edge of the linked square pyramids - which is 2.162 Å and 2.138 Å respectively; this is related to the lower electrostatic repulsion between the Oxygen species in [B] than in [A].

Concerning the macroscopic properties, we must distinguish carefully the results with the potentials. Due to the use of partial charges in set [B], the comparison with the experimental lattice energy (*i.e.* Born-Haber cycle - see Table 5 for values) is *only valid with* set [A] and [C]. Notwithstanding the large uncertainty of the second electron affinity of oxygen [39], the calculated lattice energy is too low. Such poor agreement signifies that there is a significant degree of covalence in V_2O_5 [40].

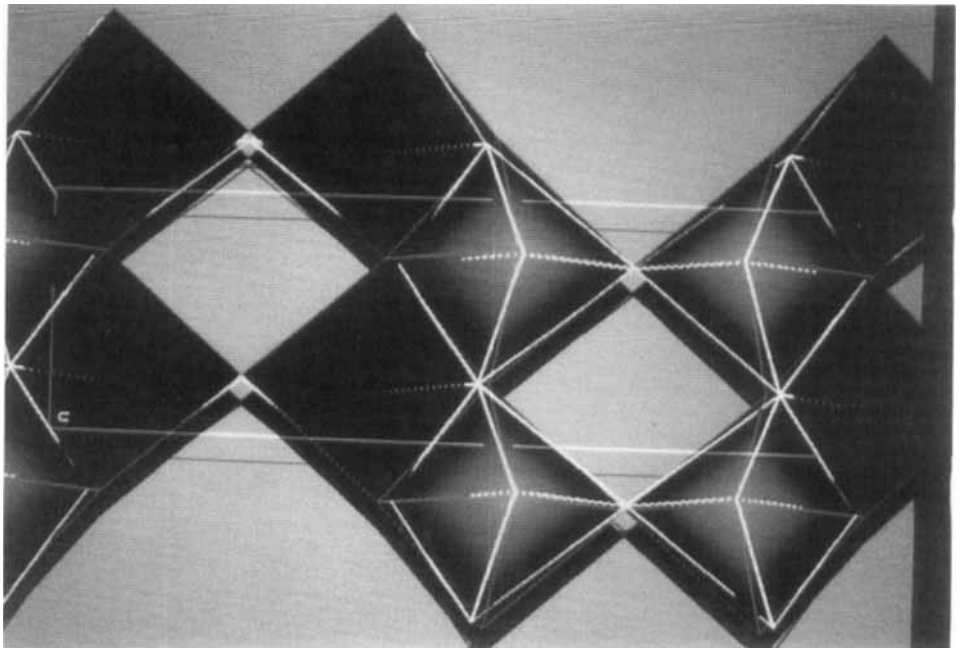

Figure 7 View along *c* axis of the observed and predicted structures. (See Colour Plates)

Table 5 Values for the experimental Lattice Energy.

Step in Born-Harber Cycle		*kcal/mole*
Heat of formation [45]	ΔH_f°	−370.60
Sublimation energy of Vanadium [37]	L	122.12
Fifth ionization potential of Vanadium [37]	I_V	3750.41
Dissociation energy of O_2 [37]	D_H	119.016
Affinity of Oxygen for two electrons [39]	E_A	140 − 210
Lattice Energy	$U_L = \Delta H_f^\circ - 2L - 5/2D_H - 2\ I_V - 5\ E_A$	
	$-9463.2 < U_L < -9113.2$	

The low frequency dielectric constants calculated with the rigid ion model reflect the polarization which occurs in the solid when the electric field displaces the negative and positive ions with respect to one another. This is called **ionic polarization** [41]. We are aware of only one published study which properly distinguishes the permittivity along each axis[1] of the orthorhombic unit-cell [42]. The authors argue that there is a substantial contribution to ε from ionic polarization because of the large difference between the squares of the refractive indices and the electric permittivity along the *a* and *b* axis. On comparing the experimental and calculated values, we found in Table 4 that the low value of the permittivity along the *c* axis

[1] We note that there is a frequent inversion of the *b* and *c* directions in different studies. We assume that sheets corresponds to the *ab* plane.

Table 6 Relaxation energies.

Structure		E_{rel}/eV *per unit cell*	E_{rel}/eV *per formula unit*	E_{rel}/eV *per Ti or V*
$VO_2(B)$		78.49	9.81	9.81
$TiO_2(B)$		76.73	9.59	9.59
$Na_2Ti_3O_7$		81.44	40.72	13.57
$Na_2Ti_6O_{13}$		137.69	68.85	11.47
V_2O_5	[A]	78.22	39.11	19.55
	[B]	50.44	25.22	12.61

relative to the values along *a* and *b* is fully reproduced; Chernenko & Ivon related this phenomenon to the layered nature of the sample perpendicular to this direction. Disagreement is found with the calculated ε_a which is lower than ε_b and drastically smaller than the experimental value. This anisotropic behavior of the tensor is greater in the results obtained in set [B]. Poor agreement between some calculated and experimental crystal properties is not surprising because high dielectric constants (>20) are such sensitive functions of any structural parameter [43]; this is especially true for ferroelectric crystals. We have also included ionic polarization via the shell model in order to calculate high frequency dielectric constants, ε_∞. The parameters of the force field [C] have been used. The calculated values follow well the evolution of the experimental refractive indices [44] as is clear from Table 4.

CONCLUSION

The agreement between predicted and experimental properties is satisfactory. The V_2O_5 structure shows strong deviations from the ideal model based on regular octahedra. The relaxation energy is considerable and can be compared to other predictions of the same type [4] as shown in Table 6. Relaxation arises from the need to adjust bond lengths, notably between those octahedra which share edges. This major effect is fully reproduced in this calculation.

In view of the remarkable value for the reliability factor ($R = 2\%$) for the refinement of the structure [18], it would be of considerable interest to determine the elastic constants with the same accuracy and also assess the electrical nature of this oxide such as the anisotropic conductivity and the ferro or antiferroelectric character.

Unlike the calculated lattice energy, the structure is very sensitive to the interatomic potentials, particularly the short-range components. We found it necessary to adjust two different kinds of potential functions in order to reproduce the complex low-symmetry distortions of this highly iono-covalent transition-metal oxide.

Acknowledgements

We should like to thank the Direction des Recherches, Etudes et Techniques for financial support (decision no. 87246) and the British Council for a generous grant (PAR/2501/2A). Alain Dietrich is also indebted to Julian Gale for useful discussions guidance with the use of the THBREL and CASCADE codes.

References

[1] C.R.A. Catlow and W.C. Mackrodt, *Computer Simulation of Solids*, Springer-Verlag, Berlin-Heidelberg-New York, 1982.

[2] M. Slaughter, "Chemical binding in Silicate minerals. II. Computational methods and approximations for the binding energy of complex Silicates." *Geochim. Cosmochim. Acta*, **30**, 315–322 (1966).

[3] W.R. Busing, "An Interpretation of the Structures of Alkaline Earth Chlorides in terms of Interionic Forces", *Trans. Am. Crystallogr. Assoc.*, **6**, 57–72 (1970).

[4] C.R.A. Catlow, A.N. Cormack and F. Theobald, "Structure Prediction of Transition-Metal Oxides using Energy-Minimization Techniques", *Acta Cryst.*, **B40**, 195–200 (1984).

[5] C.R.A. Catlow and G.D. Price, "Computer modelling of solid-state inorganic materials", *Nature*, **347**, 243–248 (1990).

[6] C.R. Walk, "Lithium-Vanadium Pentoxide Cells, in *Lithium Batteries*", Academic Press, London, 1983, pp. 265–280.

[7] A. Hardy, J. Galy, A. Casalot and M. Pouchard, "Vanadium bronzes of the formula $M_xV_2O_5$", *Bull. Soc. Chim. Fr.*, **262**, 1055–1060 (1965).

[8] J. Galy and A. Hardy, "Les bronzes $Li_xV_2O_5$. Structure cristalline de la phase monoclinique $Li_{0.30}V_2O_5$", *Bull. Soc. Chim. Fr.*, **11**, 2808–2811 (1964).

[9] J. Galy, J. Darriet and P. Hagenmuller, "Les bronzes $Li_xV_2O_5$. Structure de la phase β' et affinement de la structure de la phase γ", *Revue de Chimie minérale*, **8**, 509–522 (1971).

[10] R.J. Cava, "The structure of the Lithium-Inserted Metal Oxide δLiV_2O_5", *J. Solid State Chem.*, **65**, 63–71 (1986).

[11] P.G. Dickens, S.J. French, A.T. Hight and M.F. Pye, "Phase Relationships in the Ambient Temperature $Li_xV_2O_5$ System ($0.1 < x < 1.0$)", *Mat. Res. Bull.*, **14**, 1295–1299 (1979).

[12] M. Bose and A. Basu, "^{51}V NMR of the Layered δ-Li V_2O_5". *Journal of Solid State Chemistry*, **81**, 30–34 (1989).

[13] P.G. Dickens and M.F. Pye, "Oxide Insertion Compounds", in *Intercalation Chemistry*. Academic Press, London, 1982, pp. 539–561.

[14] R. James, "PhD Thesis", University of London (1979).

[15] F. Theobald, R. Cabala and J. Bernard, "Structure of vanadium dioxide (B)", *J. Solid State Chem.*, **17**(4), 431–438 (1976).

[16] J.A.A. Ketelaar, "Crystal structure and colloid-chemical properties of vanadium pentoxide", *Nature*, **137**, 316 (1936).

[17] A. Byström, K.A. Wilhelmi and O. Brotzen, "Vanadium Pentoxide - a Compound with Five-Coordinated Vanadium Atoms", *Acta Chem. Scand.*, **4**, 1119–1130 (1950).

[18] R. Enjalbert and J. Galy, "A refinement of the structure of V_2O_5", *Acta Cryst.*, **C42**, 1467–1469 (1986).

[19] A.R. West, *Basic Solid State Chemistry*. John Wiley & Sons Ltd, Chichester, 1988, pp. 71.

[20] J.-C. Bouloux and J. Galy, "Les Hypovanadates MV_3O_7 (M = Ca, Sr, Cd)", Structure Cristalline de CaV_3O_7. *Acta Cryst.*, **B29**, 269–275 (1973).

[21] C.A. Vincent, *Modern Batteries*. Arnold Ltd, London, 1984, pp. 165.

[22] A.D. Wadsley, "The Crystal Chemistry of Non-Stoichiometric Compounds", *Rev. Pure Appl. Chem.*, **5**, 165–193 (1955).

[23] A.D. Wadsley, "Inorganic non-stoichiometric compounds", in *Non-Stoichiometric Compounds*. Academic Press, New York, 1964, pp. 98–209.

[24] O.T. Sorensen, "Thermodynamic and Defect Structure of Nonstoichiometric Oxides", in *Nonstoichiometric Oxides*. Academic Press, New York, 1981, pp. 2–59.

[25] P.P. Ewald, "Die Berechnung optischer und elektrostatischer Gitterpotentiale", *Ann. Physik*, **64**, 253–287 (1921).

[26] M. Tosi, "Cohesion of ionic Solids in the Born model", in *Solid State Phys.* F. Seitz and S. Tumbull eds., 1964, pp. 1–120.

[27] B.G. Dick and A.W. Overhauser, "Theory of Dielectric Constants of Alkali Halide Crystals", *Phys. Rev.*, **112**, 90–103 (1958).

[28] C.R.A. Catlow, "Computer Modelling of Ionic Crystals", *J. Phys. Colloq. C6*, **41**(7), 53–60 (1980).

[29] L. Nanai and W. Volken, "Sound speed anisotropy of V_2O_5 single crystals determined by laser generated acoustic waves", *Solid State Comm.*, **70**(2), 223–224 (1989).

[30] CASCADE Program developed at HARWELL and DARESBURY and owned by the UKAEA and the SERC.

[31] R. Fletcher and M.J.D. Powell, "A Rapidly Convergent Descent Method for Minimization", *Computer J.*, **6**, 163–168 (1963).
[32] J.M. Cocciantelli, K.S. Suh, J. Sénégas, J.P. Doumere, J.L. Soubeyroux, M. Pouchard and P. Hagenmuller, "^{7}Li NMR in Electrochemically Intercalatedy γ-$Li_xV_2O_5$ Bronzes ($0.95 \leqslant x \leqslant 1.9$)", *J. Phys. Chem. Solids*, **53**(1), 51–55 (1992).
[33] W. Lambrecht, B. Djafari-Rouhani, M. Lannoo and J. Vennick, "The energy band structure of V_2O_5: I. theoretical approach and band calculations", *J. Phys. C*, **13**, 2485–2501 (1980).
[34] C.R.A. Catlow, "Point defect and electronic properties of uranium dioxide", *Proc. Roy. Soc.*, **A353**, 533–561 (1977).
[35] G.V. Lewis and C.R.A. Catlow, "Potential models for ionic oxides", *J. Phys. C*, **18**, 1149–1161 (1985).
[36] L. Abello, E. Husson, Y. Repelin and G. Lucazeau, "Vibrational spectra and valence force field of crystalline V_2O_5", *Spectrochimica Acta*, **39A**(7), 641–651 (1983).
[37] CRC, *R.C. Weast (editor)*, *Handbook of Chemistry and Physics*, C.R.C. Press, 1986–1987 67th edition.
[38] A. Dietrich and B. Maigret, "Program for the visualization of inorganic crystals", *J. Mol. Graph.*, **9**(2), 85–90 (1991).
[39] S. Cantor, "Lattice energies of cubic alkaline-earth oxides". Affinity of oxygen for two electrons. *J. Chem. Phys.*, **59**(9), 5189–5194 (1973).
[40] D.F. Shriver, P.W. Atkins and C.H. Langford, *Inorganic Chemistry*, Oxford University Press, Oxford, 1990, pp. 127.
[41] H.M. Rosenberg, "*The Solid State*", Oxford University Press, Oxford, 3rd ed., 1988, pp. 217.
[42] I.M. Chernenko, and A.I. Ivon, "Electric permittivity of vanadium pentoxide", *Sov. Phys. Solid State*, **16**(7), 1391–1392 (1975).
[43] S.M. Tomlinson, C.R.A. Catlow, H. Donnerberg and M. Leslie, "Deriving an empirical potential for ferroelectric $LiNbO_3$", *Mol. Sim.*, **4**, 335–339 (1990).
[44] N. Kenny, C.R. Kannewurf and D.H. Whitmore, "Optical absorption coefficients of vanadium pentoxide single crystals", *J. Phys. Chem. Solids*, **27**, 1237–1246 (1966).

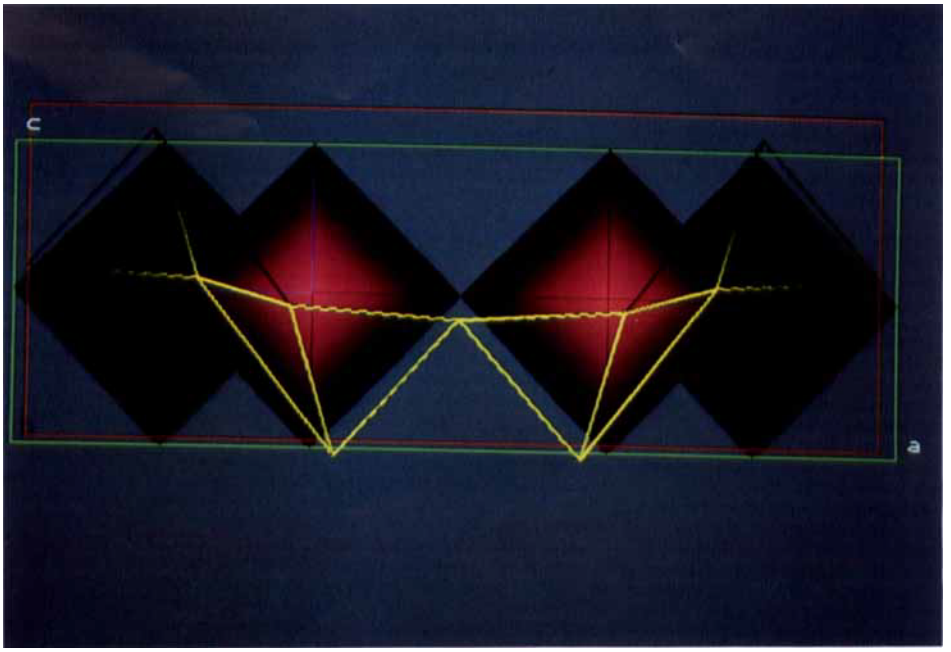

Colour Plate 1 (See Figure 5. Dietrich. pp. 251-265)

Figure 5. View along the *b* axis of the ideal structure (red facets) and the predicted one (yellow lines).

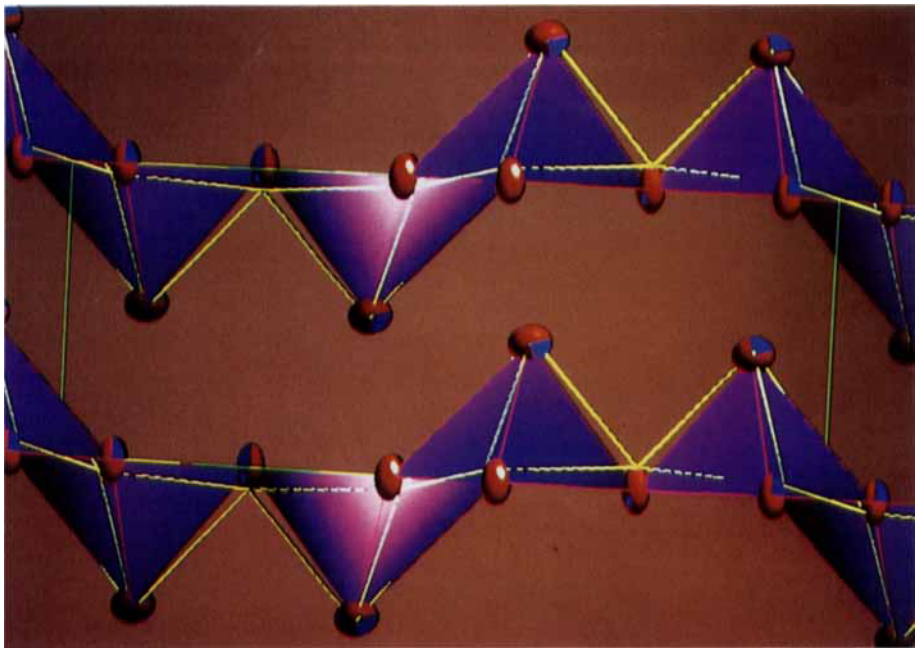

Colour Plate 2 (See Figure 6. Dietrich. pp. 251-265)

Figure 6. Comparison of the experimentally determined structure (red facets) and the predicted structure (yellow lines).

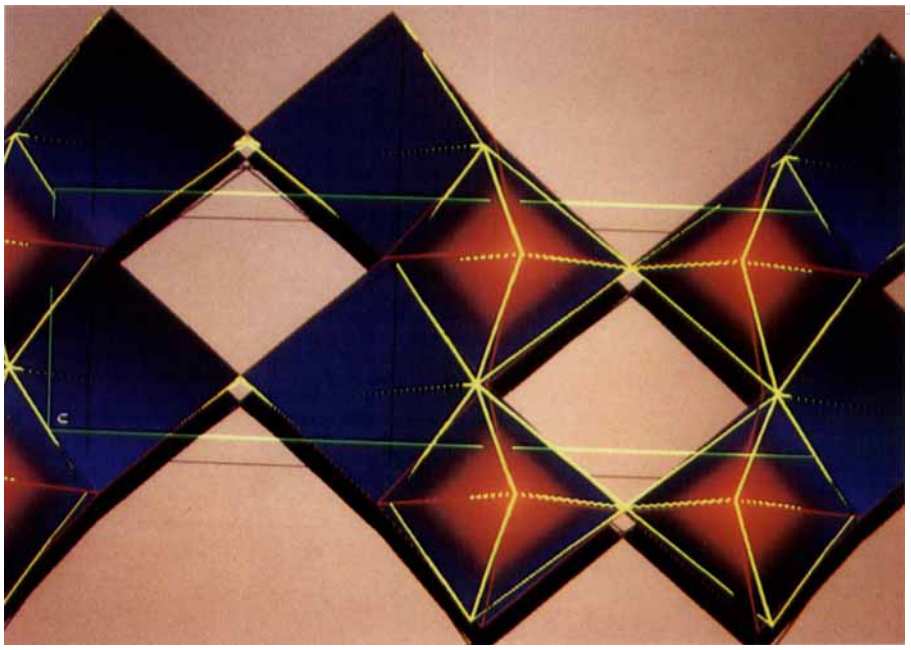

Colour Plate 3 (See Figure 7. Dietrich. pp. 251-265)

Figure 7. View along *c* axis of the observed and predicted structures.